

# Submicrometer Spatial Resolution of Metal-Enhanced Fluorescence

VINCENT J. PUGH,\* HENRYK SZMACINSKI, WAYNE E. MOORE, CHRIS D. GEDDES, and JOSEPH R. LAKOWICZ

*Microcosm, Inc., 9140 Guilford Rd., Suite O, Columbia, Maryland 21046-2585 (V.J.P., H.S., W.E.M.); Institute of Fluorescence and Center for Fluorescence Spectroscopy, Medical Biotechnology Center, University of Maryland Biotechnology Institute, 725 West Lombard Street, Baltimore, Maryland 21201 (C.D.G.); and Center for Fluorescence, University of Maryland School of Medicine, Department of Chemistry and Molecular Biology, 725 West Lombard Street, Baltimore, Maryland 21201 (J.R.L.)*

Enhanced fluorescence emission intensity from fluorescein was observed on glass slides covered with thin films of silver nanoparticles using a confocal laser-scanning microscope. The silver nanoparticle film increased the emission intensity of fluorescein by an average of at least three-fold in the area studied. Statistics are given on the enhancement of individual areas of the silver particle film with a resolution of approximately 210 nm. A histogram of intensity values indicates that the enhancement appears to occur without distinct subpopulations, with the exception that very high intensity subpopulations may occur but could not be resolved. Spatial features with dimensions near or smaller than the resolution limit of the confocal microscope, on the silver nanoparticle slide that enhanced the emission of fluorescein, were found using autocorrelation functions. These spatial features are of the same size as those found from the emission of slides containing silver nanoparticles only. These spatial features do not appear in control slides containing fluorescein without any silver nanoparticles. No long-range spatial ordering of the fluorescence enhancement on chemically deposited silver nanoparticle slides was detected.

Index Headings: Metal-enhanced fluorescence; MEF; Surface-enhanced fluorescence; SEF; Nanoparticles; Silver; Confocal; Fluorescence; Microscopy.

## INTRODUCTION

Metal-enhanced fluorescence (MEF) is the increase in fluorescence emission intensity of fluorescent molecules near metallic nanoparticles. Thin layers of metal nanoparticles have proven to be effective in increasing the emission intensity of fluorescent dyes by many groups and only a partial listing is given in the references.<sup>1-11</sup> The ability to obtain higher emission intensities from target fluorophores may offer the possibility of improvements to current fluorescence-based technologies such as DNA sequencing, immunoassays,<sup>12</sup> fluorescence *in situ* hybridization, and microarrays. In fact increased luminescence from microarray slides and improved signal-to-noise ratios have already been reported.<sup>5</sup> The increase in the luminescence signal from reporter dyes can lead to lower detection limits for many of these fluorescence-based biological assays.

Nanoparticles also reduce the emission lifetime of nearby fluorescent species as they increase the emission intensity. The ability to reduce the fluorescence lifetime and increase the quantum efficiency of a fluorescent dye, in a controlled way, is called radiative decay engineering,

which refers to the increased rate of radiative decay for fluorophores near metal particles.<sup>12</sup> Such control of the emission properties can be very useful and can, for example, lead to brighter dyes that have the ability to absorb and emit photons more quickly so that saturation and excited-state reactions are reduced.

The exact amount of emission intensity enhancement from sample to sample and between research groups does vary, sometimes significantly. This paper analyzes one source of the variation in the luminescence enhancement. The spatial variation in the luminescence enhancement of chemically prepared silver nanoparticle slides is studied with submicrometer resolution on a confocal laser-scanning microscope (CLSM). The large variations in luminescence enhancement found can be rationalized using current models of the nanoparticle-based emission enhancement.

Metal nanoparticles are expected to have several effects on the emissive properties of nearby fluorescent materials. At short distances (<5 nm) silver nanoparticles tend to quench the emission intensity of fluorescent molecules. This short-range luminescence quenching interaction has been attributed to an electrical dipole-induced-dipole interaction between the fluorophore and the silver nanoparticle.<sup>13</sup> A spacer layer between the silver nanoparticles and the fluorophore can reduce or effectively eliminate the strong quenching interaction. At slightly longer distances the emission enhancement can be modeled by supposing that the silver nanoparticle creates a locally enhanced electrical field.<sup>3,14-16</sup> The overall effect of the metal particle(s) is to increase the effective absorption coefficient and the radiative and non-radiative decay rates of the nearby fluorescent molecule. In general, this local field enhancement is a rapidly changing function of distance and orientation of the fluorophore with respect to one or more metal nanoparticles. The locally enhanced field attributable to a single metal nanoparticle drops off rapidly over a few particle lengths. This means that the enhancement associated with single metal nanoparticles drops off sharply past about 100 nm for the particles in this study. Figure 1 schematically illustrates the expected distance dependence of the quenching and enhancing interactions for an orientationally averaged sample of fluorophores near a single metal nanoparticle. While theoretical predictions have been achieved for some ideal MEF systems<sup>3,14-16</sup> and experimental data on the distance dependence of MEF has been gained for a few particular experimental systems,<sup>16,17</sup> our experimental

Received 15 January 2003; accepted 15 July 2003.

\* Author to whom correspondence should be sent. E-mail: vpugh@microcosm.com.

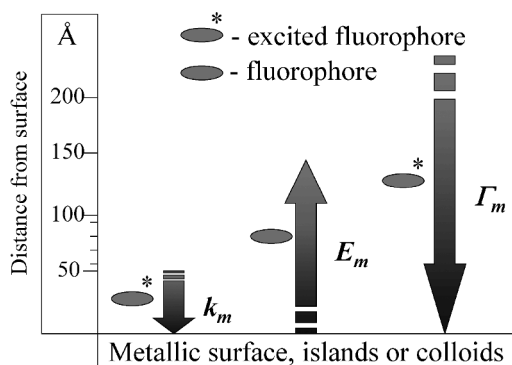


FIG. 1. Predicted distance dependencies for a metallic surface on the transitions of a fluorophore. The metallic surface can cause (electrical dipole-induced-dipole) quenching with a rate  $k_m$ , can concentrate the incident field,  $E_m$ , and can increase the radiative decay rate,  $\Gamma_m$ .

system differs from these cases. Thus, our current knowledge of the distance dependence illustrated in Fig. 1 is only an approximation.

The enhanced local fields associated with the nanoparticles lead to enhanced emission intensity from nearby fluorophores in two main ways. The first way is through an increase in the effective absorption coefficient of the molecule. The absorption rate of a molecule is proportional to the electric field strength squared. Hence, increasing the local field strength at the excitation frequency leads to an increased absorption coefficient and rate. The second way is by increasing the radiative rate of a fluorophore, which results in increasing the quantum yield and decreasing the lifetime. An increasing quantum yield with a decreasing emission lifetime is inherent to MEF though it is unusual in the sense that quantum yields and emission lifetimes both increase or decrease together under most circumstances.

In addition to the single nanoparticle effects that can enhance luminescence, multiparticle effects can also play a role in enhancing the luminescence of nearby fluorophores. The electric-field enhancement can be increased if nanoparticles are near to each other and the particles cooperatively increase the local electric field.<sup>15</sup> The effects of multiple particles on the field enhancement are expected to be significant, and spatially resolved measurements of luminescence enhancement will be needed to help experimentally determine the arrangement of nanoparticles required to maximize the metal-enhanced fluorescence.

Statistical analysis of high-resolution images of slides where metal-enhanced fluorescence occurs allows a greater understanding of some features of the enhancement process in this format. This high spatial resolution allows a number of questions about MEF in these systems to be addressed. The following questions will be focused on here: “Are there distinct subpopulations of nanoparticles that enhance emission differently?”; “Are there structures that give particularly high MEF in the colloidal silver film (CSF) slides?”; “Are there periodic or semi-periodic structures in the nanoparticle films that affect the MEF?”; “What are some of the greatest enhancements that can be expected?”

Histograms of pixel intensities measured over a large spatial area can address the question of whether distinct

subpopulations exist for MEF in the sample examined. The histogram may also be of use in determining the maximum amount of enhancement that can be expected. It may be possible to engineer materials that display the amount of MEF shown at the peak of the intensity distribution. Other questions about the spatial distribution in the degree of MEF require other statistical image analysis techniques.

The question of spatial periodicity, the degree of metal-enhanced fluorescence in CSFs, is relevant as some nanoparticle films prepared by vacuum techniques are reported to have spatial periodicity in the location of CSFs.<sup>10</sup> The spatial periodicity of chemically deposited nanoparticle films (as described further below) and specifically the spatial periodicity (if any) of the luminescence enhancement by these chemically deposited films are explored here. The use of a confocal laser-scanning microscope allows testing for periodic or semi-periodic features with periods that are longer than the resolving power of the microscope.

Autocorrelation functions display feature sizes and spatial periodicities in images, ultimately allowing questions of feature size and spatial periodicity in the MEF of CSFs to be addressed. The autocorrelation function is a particularly useful image analysis tool for images where there are many bright pixels, such as some of the images acquired using the CLSM (see further below). For these types of images, the autocorrelation function can give indications of feature sizes, whereas other image analysis tools, such as feature size analyses, fail for images containing many bright pixels. The autocorrelation function is used as a main image analysis technique here because bright images are to be analyzed and compared.

An autocorrelation function for the intensity (differences from the average) can be defined as:

$$A(j) = \sum_{i=0}^{N-j-1} [I(i) \times I(i+j) - I_{\text{AVG}} \times I_{\text{AVG}}] \quad (1)$$

$A(j)$  is the autocorrelation function for pixels separated by distances of  $j$  pixel units.  $I(i)$  is the intensity of pixel  $i$  and  $I(i+j)$  is the intensity of the pixel  $i+j$  where the pixels are ordered sequentially along one axis.  $I_{\text{AVG}}$  is the average pixel intensity value over the axis. For the analysis to follow, the average of autocorrelation functions across each line of an image is taken.

The action of the line-averaged autocorrelation function on an image can be visualized by performing the following mental operations on an image: (1) duplicate the image, keeping the duplicate image slightly above the original but not displaced from side to side; (2) shift the duplicate image to the right or left by  $j$  pixels; (3) create a new image by multiplying the intensities of the original and shifted images for each set of two corresponding pixels; (4) subtract the (squared) average pixel intensity of the original image from the calculated image and sum the leftover values; (5) repeat for all valid values of  $j$ . This last description applies to taking the autocorrelation function in the horizontal direction (side-to-side). The autocorrelation function in the vertical direction can be taken by shifting the duplicate image up or down rather than to the right or left.

The ability of the autocorrelation function to indicate

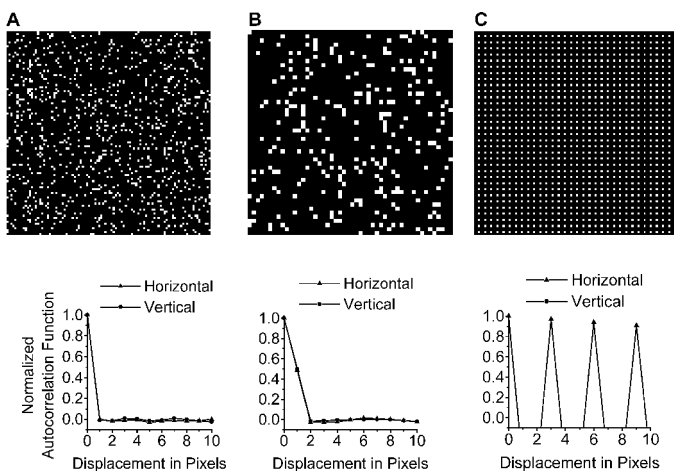


FIG. 2. The images are computer simulated. Each image was generated by placing bright pixels onto a black  $100 \times 100$  pixel image. Image (A) was generated by randomly placing 1000 bright single pixels. Image (B) was generated by randomly placing 250 blocks of  $2 \times 2$  bright pixels. Image (C) was generated by placing bright pixels in a square grid, with two black pixels remaining between each bright pixel both horizontally and vertically. The averaged autocorrelation functions for each image are shown immediately below that image. The directions in which the autocorrelation functions are taken, either in the horizontal or vertical directions, are given in the legend in each graph.

spatial features is illustrated in Fig. 2. The simulated image in Fig. 2A is of randomly distributed single pixels. The autocorrelation function for this image shows no periodicity, nor any value (significantly) above zero beyond zero displacement. The image in Fig. 2B is of randomly distributed two-by-two pixel blocks. The autocorrelation function associated with this image shows significant magnitude at values greater than zero, indicating spatial features with sizes above one pixel. The autocorrelation functions for these randomly distributed features show no peaks at pixel displacement beyond zero. In contrast, the autocorrelation function for the periodic structure image shown in Fig. 2C does show characteristic peaks beyond zero displacement. The forms of the autocorrelation functions in Fig. 2 reflect the underlying data and can be rationalized by carrying out the mental operations outlined previously.

The autocorrelation function with respect to pixel displacement can be converted to the autocorrelation function with respect to displacement in nanometers by changing the variable using the width (or height) of the pixels in nanometers, for estimation of image size features. It must be noted, however, that the size of the features discernable from the autocorrelation function of images is limited by the resolution of the microscope. The autocorrelation function of intensity vs. position from the measurement is the autocorrelation function of intensity vs. position for infinite resolution convolved with the point-spread function of the microscope. This means that features below the resolution of the microscope will be smeared out in the measured autocorrelation function. Features in the autocorrelation function with lengths well above the resolution of the microscope will only be slightly broadened.

## MATERIALS AND METHODS

Nanoparticulate silver film slides were prepared as described in the literature except that Corning glass cover

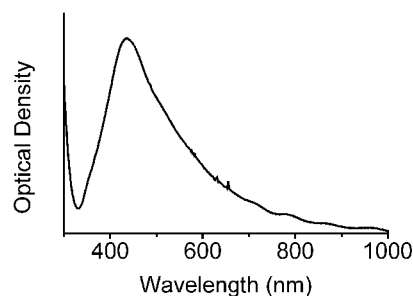


FIG. 3. A typical optical density plot for silver nanoparticles on glass slides.

slides were used rather than quartz slides.<sup>1</sup> The preparation technique for the CSF slides involves creating colloidal silver particles in solution with amine-coated glass cover slides. The colloidal silver adheres to the slides, or may be formed directly on the slides, and the slides with the CSF are removed from solution when a sufficiently optically dense (an optical density between 0.1 to 0.4) greenish coating of silver nanoparticles is achieved. The slides are subsequently sonicated and washed of excess coating solution.

A number of the slides were then coated with monolayers of proteins and fluorophores following reported procedures.<sup>6</sup> Bare CSF slides were first covered by a monolayer of biotinylated bovine serum albumin (BSA-biotin). Next a layer of avidin was placed over the layer of BSA-biotin. Finally, a layer of biotin-4-fluorescein was added on top of the avidin layer. Several control slides were produced. Control slides without silver nanoparticles, without fluorescein, or without silver nanoparticles and fluorescein were treated in the same fashion and kept in the same solutions as the fluorescein on protein-coated CSF slides except that the steps that would have produced the missing components were skipped. All reagents were purchased from Sigma-Aldrich and used without purification.

UV-Vis spectra of the silver nanoparticle films were taken on an HP 8453 Diode Array Spectrophotometer. The slides were examined using a Zeiss CLSM 410 with a  $63\times$  Zeiss Plan-Apochromat 1.40 NA oil objective. The fluorescein was excited with the 488 nm laser line from an argon ion laser. A dichroic emission filter with a 535 to 570 nm bandpass was used to collect emitted light. The CLSM instrumental parameters such as PMT gain, brightness, and zoom were held constant for each image. The image size was  $68 \mu\text{m}$  by  $68 \mu\text{m}$  and  $512$  by  $512$  pixels.

The data was processed in part using "Scion Image for Windows" from Scion Corporation. Histograms of pixel intensities were produced using the Scion Corp. software. The autocorrelation function analyses were performed using custom software. The autocorrelation functions were determined along the horizontal and vertical directions and are the average of the autocorrelation functions of all lines of an image. The autocorrelation function was normalized so that the highest peak value was set to a value of one.

The atomic force microscopy (AFM) of slides similar to those employed in the fluorescence experiments were performed with a Nanoscope IIIa (Digital Instruments).

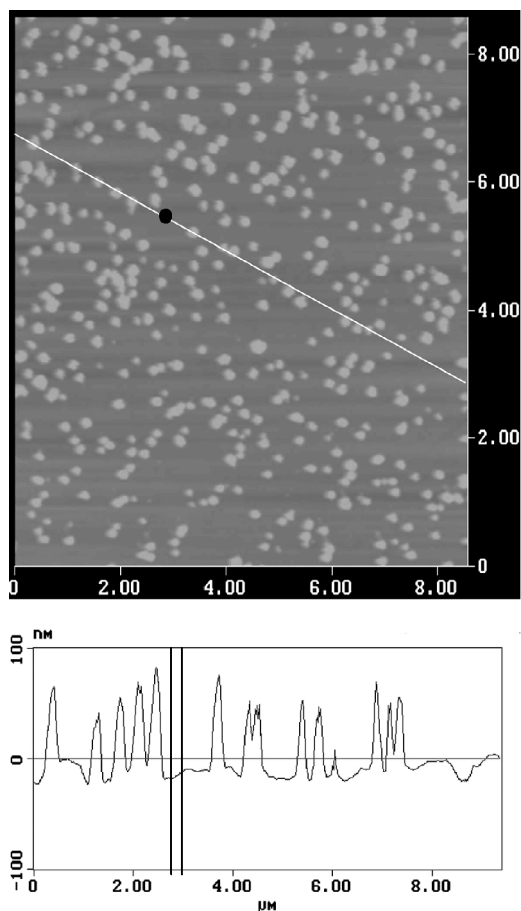


FIG. 4. AFM of silver nanoparticles on an amine-coated quartz slide. The bright line indicates the source of the surface height profile given in the graph immediately below the AFM image. The black dot located on the line indicates the approximate size of the focal spot of the CLSM. The two black lines in the height profile graph indicate the diameter of the CLSM focal spot.

The AFM probes used were silicon nitride and had nominal spring constants of 40 N/m and resonant frequencies near 170 kHz.

## RESULTS AND DISCUSSION

The CSF slides have moderately high densities of silver particles. A characteristic spectrum of the optical density of CSF is shown in Fig. 3. The optical density of the CSF is fairly high, near 0.1. This partial monolayer of silver nanoparticles absorbs or scatters a significant fraction of the incoming light at the peak of the plasmon

resonance associated with the silver particles. The form of the optical density spectrum is typical for small (on the order of tens of nanometers) silver particles. Additionally, from the AFM images (Fig. 4) it can be seen that the silver particles cover a significant fraction of the surface area of the slide, so that the CSFs have a moderate density of surface coverage. The AFM images also indicate that the chemically deposited silver nanoparticles have variations in size and distribution. The data for Figs. 3 and 4 are representative only and not directly from the imaged slides; however, the imaged slides were produced in a way that was very similar to the samples from which Figs. 3 and 4 were created. Figure 5 shows a schematic diagram of the physical layout of the slides that display MEF.

The (Rayleigh) resolution of a diffraction limited confocal microscope is:<sup>16</sup>

$$\delta_r \cong 0.61 \frac{\lambda}{NA} \quad (2)$$

where  $\delta_r$  is the diameter of the resolved spot,  $\lambda$  is the wavelength of the light, and  $NA$  is the numerical aperture. Thus, the resolving power of the CLSM in the plane parallel to the surface of the CSF is expected to be around 210 nm. The spatial region with the maximum emission enhancement from small numbers of nanoparticles is expected to vary rapidly and rise to a peak within a few nanoparticle diameters, if not closer (<100 nm), and then rapidly fall (see Fig. 1). The resolution of the CLSM is too low to observe the sharp dependence of the luminescence enhancement on the distance of a fluorophore from a nanoparticle. However, the CLSM has sufficient resolution to determine the overall enhancement from just a few silver nanoparticles. The previously calculated size of the focal spot of the CLSM is indicated on Fig. 4.

The ability to probe the luminescence enhancement locally allows a way to find optimal areas of enhancement. These areas occur where the size and spatial arrangement of the nanoparticles is optimal. The shape of nanoparticles is also known to be important<sup>15</sup> and may play a significant role in the variation of the MEF even within the same slide. The results for small areas can be used to find the maximum enhancement that can be achieved for a given particle and fluorophore configuration, that is, optimal nanoparticle shape and size with a given fluorophore spacing and density. For the current experiments, the spacing between the fluorophore and the nanoparticle is fixed near 8 nm by the protein layer. The fluorophore

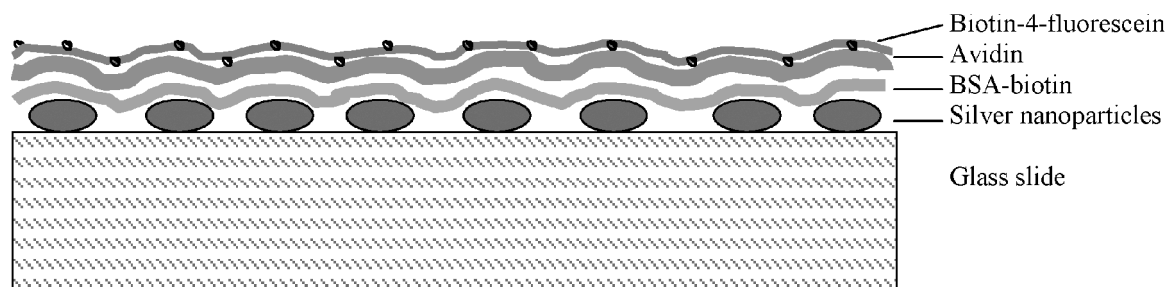


FIG. 5. Schematic diagram indicating the location of the different layers on the slide that displayed the MEF. The relative sizes of features in the figure are not to scale.

**A—Fluorescein-protein-silver**    **B—Fluorescein-protein**    **C—Protein-silver**

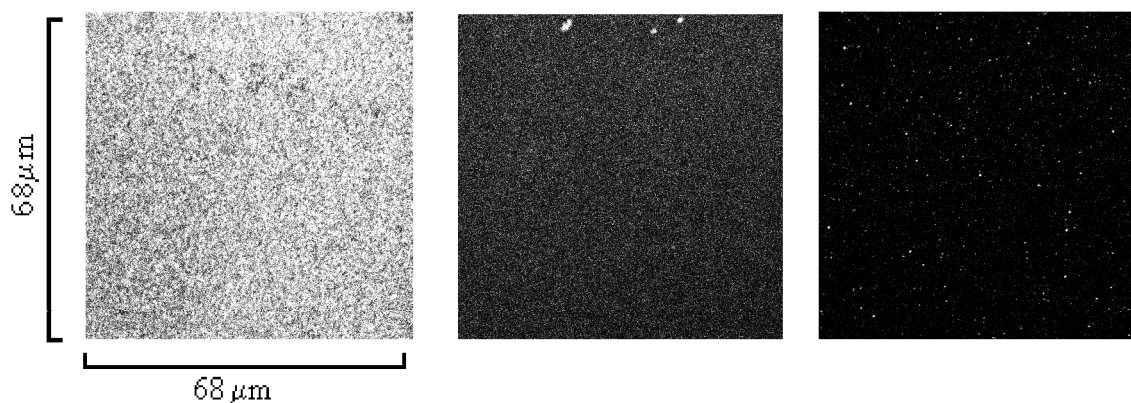


FIG. 6. Images were taken on a Zeiss 410 CLSM using 488 nm excitation with instrumental parameters kept constant for each image. Each image contains  $512 \times 512$  pixels. (A) Fluorescein attached to a protein layer over a silver nanoparticle layer. (B) Fluorescein attached to a protein layer without silver nanoparticles. (C) A protein and silver nanoparticle layer without attached fluorescein.

surface density is estimated to be below a monolayer at approximately  $1.1 \text{ pmol/cm}^2$ .

Images from three slides showing MEF of fluorescein and control slides are shown in Fig. 6. Figures 6A, 6B, and 6C show images from a fluorescein–protein–CSF slide, fluorescein–protein slide, and protein–CSF slide, respectively. Overall, the average emission intensity enhancement for fluorescein is about 3 (from Fig. 6) and is consistent with the eight-fold intensity enhancement obtained by Sokolov et al.<sup>6</sup> for similar samples, given that many pixels were saturated in the MEF image (Fig. 6A).

In Fig. 7 are shown histograms of intensity distributions within each image. The histograms in Fig. 7 were obtained directly from the images shown in Fig. 6. Histogram values corresponding to zero intensity and saturated intensity (255) are excluded from Fig. 7 in order to accommodate comparisons between images. Percentage values are given for each histogram indicating the fraction of the total number of pixels in the image that are represented in the histogram. Graphs showing the number of saturated intensity and zero intensity pixels for each slide are displayed separately in Fig. 8. The histograms show clearly distinct distributions of fluorescence intensity in the three images. In the fluorescein with CSF image (Fig. 6A) there are a large number of pixels with intensities above the value of 200, whereas for the fluorescein image without any silver nanoparticles most of the pixel intensities are lower than 200; the intensity dis-

tribution is shifted from low intensity values (Fig. 6B) to higher intensity values (Fig. 6A). The control sample (Fig. 6C) shows that CSF covered with a protein layer has a low background compared to those with fluorescein (Fig. 6A and Fig. 6B). The histograms do not indicate any distinct subpopulations in the MEF for modest enhancements, which give fluorescence within the dynamic range of the instrument.

The Zeiss CLSM 410 using Zeiss software reports eight bits of intensity data for each pixel (measured intensity values range from 0 to 255). A large number of the pixels in the images showing fluorescence enhancement by the silver nanoparticles were saturated because the same microscope settings had to be used for the control slides and for the metal-enhanced fluorescence to accommodate comparison and quantitative calculations. Figure 8 shows charts indicating the number of saturated pixels in each image. The clipping of the intensity values at the saturation value leads to an underestimation of the true fluorescence enhancement by the CSF. A three-fold increase in the fluorescence of fluorescein from the CSFs was derived from comparing the average pixel intensities of the appropriate images, with the instrumental saturation limit on the pixel intensities. The actual fluorescence enhancement is likely considerably higher if the average intensity of saturated pixels is higher than the value of 255. Additionally, the saturation limit makes it impossible to distinguish between subpopulations of enhance-

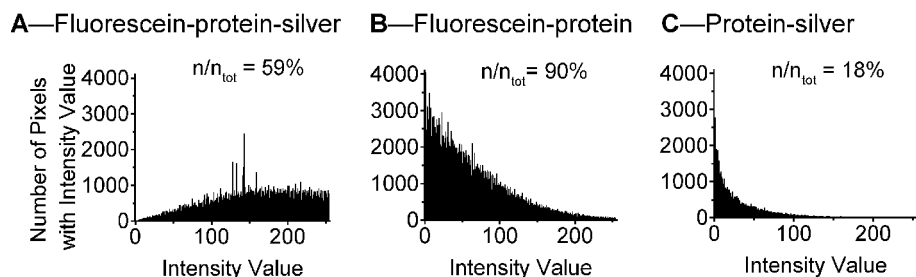


FIG. 7. Histograms of the pixel intensities of the images in Fig. 6. The histograms indicate the number of pixels with a particular intensity count (1 to 254) in the image. The histogram values for zero intensity and saturated intensity are omitted here for clarity. The histograms labeled A, B, and C correspond to the images shown in Figs. 6A, 6B, and 6C, respectively. There are 262 144 total pixels in each of the  $512 \times 512$  pixel images and the percentage of the total pixels represented on each histogram is given by the  $n/n_{\text{tot}}$  value on the graphs.

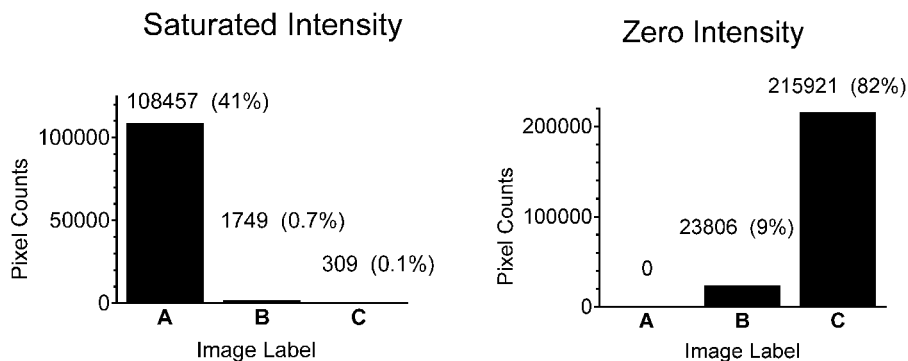


FIG. 8. Charts indicating the number of (left) intensity saturated and (right) zero intensity pixels in the respective images displayed in Fig. 6. There are 262 144 pixels in each image. The number of pixels associated with each bar is given immediately to the right of the bar.

ment regions where the enhanced fluorescence is greater than the saturation limit. It is clear, however, that some regions of the slide appear to be much brighter than others and further study will be needed to reveal precise conditions necessary to maximize the MEF so that all areas of the slide experience the same enhancement as the bright areas found.

Importantly, the number of saturated intensity pixels is much larger (about 62-fold) for the silver-enhanced image (Fig. 6A) compared to the image without silver (Fig. 6B). The chart with zero intensity pixels (Fig. 8, right) also confirms the enhancement by indicating no zero intensity pixels as compared to about 9% zero intensity pixels for the fluorescein image without silver. Moreover, the noise contribution for the silver nanoparticles alone is very small, with only 0.1% of total pixels showing saturated intensity and 82% showing zero intensity for the images of silver nanoparticles alone.

The average autocorrelation of intensity vs. pixel displacement along the horizontal and vertical axes in each of the images is shown in Fig. 9. This autocorrelation function indicates the spatial lengths and length distributions of intensity features in the images. The autocorrelation functions in the horizontal and vertical directions are equivalent within measurement uncertainty, which indicates that there are no features that are preferentially oriented either vertically or horizontally in the images.

Intensity images from spatially uniform sources where there are no spatially varying intensity features except for random statistical variations (noise) should have spatial autocorrelation functions that peak only at zero displacement and are zero (within experimental uncertainty) for any other displacement. That is, the intensity of each pixel will be correlated with itself only and not correlated

with any of the neighboring pixels. The fluorescein layer alone is expected to show just such an autocorrelation function if it is a true uniform monolayer (within the resolution of the microscope). The spatial autocorrelation functions for fluorescein in Fig. 9B match these expectations. Note that only the autocorrelation functions for small pixel displacements (up to 5 pixels) are shown because the autocorrelation functions for larger pixel displacements are nearly zero.

The intensity-vs.-pixel-displacement autocorrelation functions for spatially small features that are randomly distributed should show a peak at zero pixel displacement and a rapidly decaying (but non-zero) autocorrelation function for higher pixel displacements that are within the size distribution of the small features. The autocorrelation function beyond the largest bright spatial feature in the image should go to zero (within experimental uncertainty). This is the case for both images with CSFs. The intensity-vs.-spatial-displacement autocorrelation functions are very similar for both the fluorescence from the fluorescein enhanced by the CSFs and the background signal from silver nanoparticles alone. This implies that the features that give rise to the metal-enhanced fluorescence and the silver-nanoparticles background are similar (if not identical) in size. In our case, these features are likely single nanoparticles or collections of nanoparticles. The implication from the image analysis that the silver nanoparticles are responsible for the weak background luminescence in the absence of fluorescein is consistent with recent findings that silver nanoparticles emit light under intense excitation.<sup>19</sup>

The intensity features in the silver-nanoparticle-containing slides are only a few pixels in width, close to the resolving power of the microscope (210 nm or about 1.5

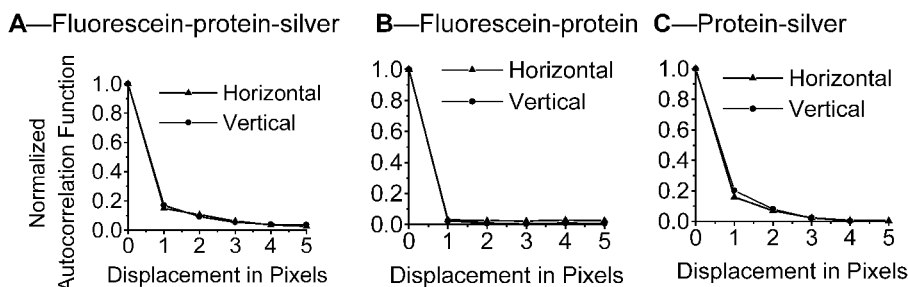


FIG. 9. Average normalized intensity vs. pixel distance autocorrelation functions for the images in Fig. 6. The data for the autocorrelation functions labeled A, B, and C in this figure were taken from the respective Figs. 6A, 6B, and 6C in the horizontal and vertical directions.

pixels). Thus, it is difficult to resolve the exact size distribution of the features. However, it can be stated that the majority of intense features have characteristic lengths that are less than 4 pixels (or 560 nm).

The similarity of the sizes of the intensity features in the images with silver nanoparticles, along with the lack of discernable intensity features in the fluorescein-alone slides, indicates that the emission from almost all of the fluorescein molecules near the silver nanoparticles are affected by the silver nanoparticles. The pixel intensity distributions and the number of intensity saturated pixels also imply that the silver nanoparticles strongly affect the fluorescence of essentially all of the fluorescein molecules attached to the protein monolayer above the nanoparticles. The existence of small areas on CSF slides where the fluorescence is maximal indicates that techniques that deposit the silver nanoparticles in well-defined ways, such as bead lithography,<sup>20</sup> may result in even greater average enhancements than CSFs deposited from solutions of colloidal silver.

Intensity features in images with periodic or semi-periodic structure over long distances should show peaks in the intensity-vs.-spatial-displacement autocorrelation function. The autocorrelation functions beyond 5 pixels of displacement (700 nm) show no significant peaks. Thus, no evidence for any periodic intensity features was found in any of the images examined. This is consistent with the expectation that a partial monolayer of silver nanoparticles deposited chemically should have no long-range periodic or semi-periodic order. However, silver layers deposited by other means, such as vapor deposition, heat treating of thin silver films, or thicker layers of chemically deposited nanoparticles, may contain semi-periodic features.

## CONCLUSION

The metal-enhanced fluorescence of fluorescein on protein-coated silver nanoparticle slides was studied with submicrometer resolution. The fluorescence of fluorescein attached to a protein layer on silver nanoparticles was strongly affected. The vast majority of the fluorescein molecules appeared to be strongly affected by the presence of the silver particles from the pixel intensity data and from the autocorrelation of intensity with pixel displacement data. The three-fold overall enhancement of

the fluorescein fluorescence intensity by a silver nanoparticle film was calculated as the average over the entire image. *Substantially higher* enhancement can be estimated by correcting for intensity-saturated pixels. Small submicrometer spatial features were found in the images containing silver nanoparticles but not in the images without silver particles. No long-range periodic or semi-periodic pattern was found in any of the samples.

## ACKNOWLEDGMENTS

This work was performed with the partial support of NIH grant 1 R3 CA097569-01 and the NIH National Center for Research Resources, RR-08119.

1. J. R. Lakowicz, B. Shen, Z. Gryczynski, S. D'Auria, and I. Gryczynski, *Biochem. Biophys. Res. Comm.* **286**, 875 (2001).
2. J. R. Lakowicz, Y. Shen, S. D'Auria, J. Malicka, J. Fang, Z. Gryczynski, and I. Gryczynski, *Anal. Biochem.* **301**, 261 (2002).
3. J. Kümmerlen, A. Leitner, H. Brunner, F. R. Aussenegg, and A. Wokaun, *Mol. Phys.* 1031 (1993).
4. C. D. Geddes and J. R. Lakowicz, *J. Fluorescence* **12**, 121 (2002).
5. N. Stich, A. Gandhum, V. Matushin, C. Mayer, G. Bauer, and Th. Schalkhammer, *J. Nanosci. Nanotechnol.* **1**, 397 (2001).
6. K. Sokolov, G. Chumanov, and T. M. Cotton, *Anal. Chem.* **70**, 3898 (1998).
7. A. M. Glass, P. F. Liao, J. G. Bergman, and D. H. Olson, *Opt. Lett.* **5**, 368 (1980).
8. P. J. Tarcha, J. DeSaja-Gonzales, S. Rodriguez-Llorente, and R. Aroca, *Appl. Spectrosc.* **53**, 43 (1999).
9. T. Hayakawa, S. T. Selvin, and M. Nogami, *Appl. Phys. Lett.* **74**, 1513 (1999).
10. N. Streakal, A. Maskevich, S. Maskevich, J. Jardillier, and I. Nabiev, *Biopolymers* **57**, 325 (2000).
11. D. A. Weitz, S. Garoff, C. D. Hanson, and T. J. Gramila, *Opt. Lett.* **7**, 89 (1982).
12. J. R. Lakowicz, *Anal. Biochem.* **298**, 1 (2001).
13. A. Campion, A. R. Gallo, C. B. Harris, H. J. Robota, and P. M. Whitmore, *Chem. Phys. Lett.* **73**, 447 (1980).
14. P. Das and H. Metiu, *J. Phys. Chem.* **89**, 4680 (1985).
15. J. I. Gersten and A. Nitzan, *Surf. Sci.* **158**, 165 (1985).
16. A. Wokaun, *Mol. Phys.* **56**, 1 (1985).
17. R. Aroca, G. J. Kovacs, C. A. Jennings, R. O. Loutfy, and P. S. Vincett, *Langmuir* **4**, 518 (1998).
18. K. R. Castleman, "Sampling, Resolution, and Digital Image Processing in the Spatial and Fourier Domains", in *Confocal and Two-Photon Microscopy: Foundations, Applications, and Advances*, A. Diaspro, Ed. (John Wiley and Sons, New York, 2002), pp. 237-251.
19. C. D. Geddes, A. Parfenov, and J. R. Lakowicz, *J. Fluorescence*, paper in press (2003).
20. T. R. Jensen, M. D. Malisky, C. L. Haynes, and R. P. Van Duyne, *J. Phys. Chem. B* **104**, 10549 (2000).